Title: Spiropyran-based Nanocarrier: A New Zn2+-Responsive Delivery System with Real Time Intracellular Sensing Capabilities.

Authors: Sabrina Heng; Xiaozhou Zhang; Jinxin Pei; Alaknanda Adwal; Philipp Reineck; Brant Gibson; Mark Hutchinson; Andrew Abell

To be cited as: 10.1002/chem.201804816

Link to VoR: https://doi.org/10.1002/chem.201804816

Spiropyran-based Nanocarrier: A New Zn^{2+}-Responsive Delivery System with Real Time Intracellular Sensing Capabilities.

Sabrina Heng,[a], [b] Xiaozhou Zhang,[a], [b] Jinxin Pei,[a], [c] Alaknanda Adwal,[d] Philipp Reineck,[a], [e] Brant C. Gibson,[a], [e] Mark R. Hutchinson,[a], [c] Andrew D. Abell.*, [a], [b]

Abstract: A new spiropyran-based stimuli-responsive delivery system is presented that encapsulates and then releases an extraneous compound in response to elevated levels of Zn^{2+}, a critical factor in cell apoptosis. A C_{12}-alkyl substituent on the spiropyran promotes self-assembly into a micelle-like nanocarrier in aqueous media, with nanoprecipitation and encapsulation of added payload. Zn^{2+} binding occurs to an appended bis(2-pyridylmethyl)amine group at biologically relevant micromolar concentration. This leads to switching of the spiropyran (SP) isomer to the strongly fluorescent ring opened merocyanine-Zn^{2+} (MC-Zn^{2+}) complex, with associated expansion of the nanocarriers to release the encapsulated payload. Payload release is demonstrated in solution and in HEK293 cells by encapsulation of a blue fluorophore, 7-hydroxycoumarin, and monitoring its release using fluorescence spectroscopy and microscopy. Furthermore, we demonstrate the use of the nanocarriers to deliver a caspase inhibitor, Azure B, into apoptotic cells in response to an elevated Zn^{2+} concentration. This then inhibits intracellular caspase activity, as evidenced by confocal microscopy and in real-time by time-lapsed microscopy. Finally, the nanocarriers are shown to release an encapsulated proteasome inhibitor (**5**) in Zn^{2+}-treated breast carcinoma cell line models. This then inhibits intracellular proteasome and induces cytotoxicity to the carcinoma cells.

Introduction

Fluorescence is arguably the most powerful and widely used technique for cell-based sensing and imaging in living systems.[1] Highly sensitive and specific fluorescence-based sensors for biologically important analytes such as metal ions,[2] signaling molecules (e.g. H_2O_2 and glutathione),[3] and enzymes[4] allow the study of fundamental cell-based processes; including protein trafficking, small-molecule signaling, organelle distribution and cell viability. These processes are complex, involving an interplay of multiple chemical pathways and molecules, the concentration and activity of which are in a constant state of flux in response to both internal and external stimuli. Programmed cell death (apoptosis) is a good example, being controlled by highly interrelated intracellular regulators including Zn^{2+} and caspases 3, 6, 7, 8 and 9. These caspases induce apoptosis in mammalian cells by regulating key protein factors in the intrinsic and extrinsic apoptotic pathway. Caspase activity is tightly regulated by fluctuations in intracellular Zn^{2+} levels.[5] The concentration of cytosolic Zn^{2+} thus provides a marker for early and late apoptosis[6] and hence the development of cancer,[7] autoimmune disease (e.g. rheumatoid arthritis),[8] neurodegenerative disorders such as Parkinson's, Alzheimer's and others diseases.[9] For example, elevated intracellular levels of Zn^{2+} are associated with malignancy and invasiveness of breast tumors. Intracellular Zn^{2+} is therefore an important biomarker for the diagnosis and subsequent treatment of invasive breast cancers.[10]-[11] A real advance would come with a new nanocarrier that releases an encapsulated therapeutic agent specifically in response to Zn^{2+} binding, with concomitant sensing of the analyte and tracking of the nanocarrier by fluorescence. Here we incorporate a therapeutic or diagnostic agent (payload) into a self-assembled spiropyran-based nanocarrier as a first step towards such a stimuli-responsive delivery tool. Zn^{2+}-triggered release of the encapsulated payload and simultaneous sensing of intracellular Zn^{2+} concentration by fluorescence. The spiropyran used is readily functionalised to allow binding of Zn^{2+}.

Exposure of the spiropyran-based nanocarrier to Zn^{2+} isomerizes the component spiropyran (SP) to its ring-opened merocyanine isomer (MC)[2a, e, 12] with an associated change in polarity and geometry. We envisioned that this would result in an overall size change of the nanocarrier to release the encapsulated payload. Healthy cells possess very low concentrations of free Zn^{2+} ion (0.1 – 1 nM) insufficient to induce this isomerization. The payload thus remains trapped in the nanocarrier until exposure to elevated levels of Zn^{2+} (micromolar concentrations), as found in diseased cells.[13] Exposure of healthy cells to the payload is thus minimized, with specific delivery only occurring to diseased cells such as is required in cancer chemotherapy.[14] In addition, our approach provides a means to sense Zn^{2+} concentration at the delivery site concomitantly to the payload release. This is achieved by the switching of the nanocarriers from the non-fluorescent SP state to the highly fluorescent MC-Zn^{2+} complex upon Zn^{2+} binding. This significant increase in fluorescence allows detection of changes in intracellular Zn^{2+} concentrations (Figure 1) and also tracking of the distribution of the nanocarrier in cells.

[a] ARC Center of Excellence for Nanoscale BioPhotonics (CNBP), Institute for Photonics and Advanced Sensing, University of Adelaide.
[b] Department of Chemistry, The University of Adelaide, Adelaide, South Australia 5005, Australia.
[c] Department of Physiology, Adelaide Medical School, The University of Adelaide, South Australia.
[d] The Robinson Research Institute, Adelaide Medical School, The University of Adelaide, Adelaide SA 5005.
[e] CNBP, School of Science, RMIT University, Melbourne, Victoria, 3001, Australia.

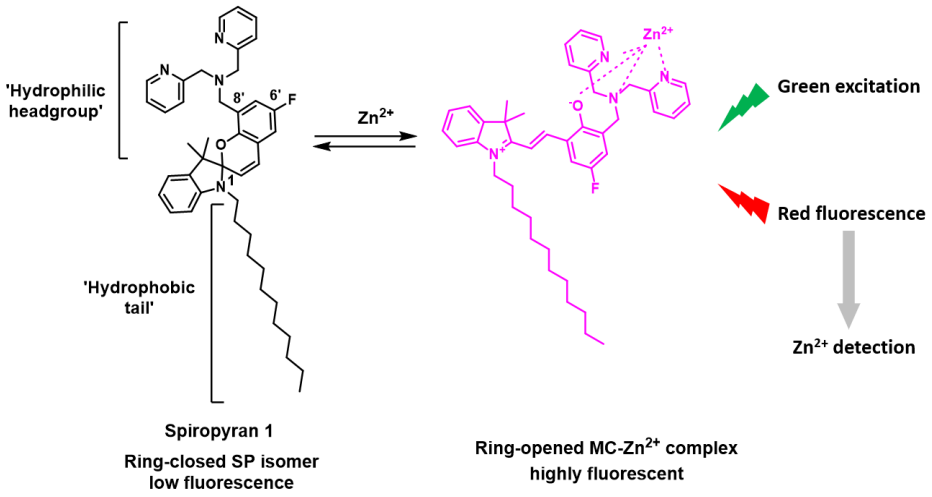

Figure 1. Interconversion of spiropyran (SP) and merocyanine (MC) isomers used to construct the spiropyran-based nanocarrier. The ring-closed spiropyran (SP) is weakly fluorescent and the Zn^{2+}-induced ring-opened merocyanine complex (MC-Zn^{2+}) is highly fluorescent. Binding of Zn^{2+} induces formation of the MC-Zn^{2+} complex with release of the encapsulated payload.

Results and Discussion

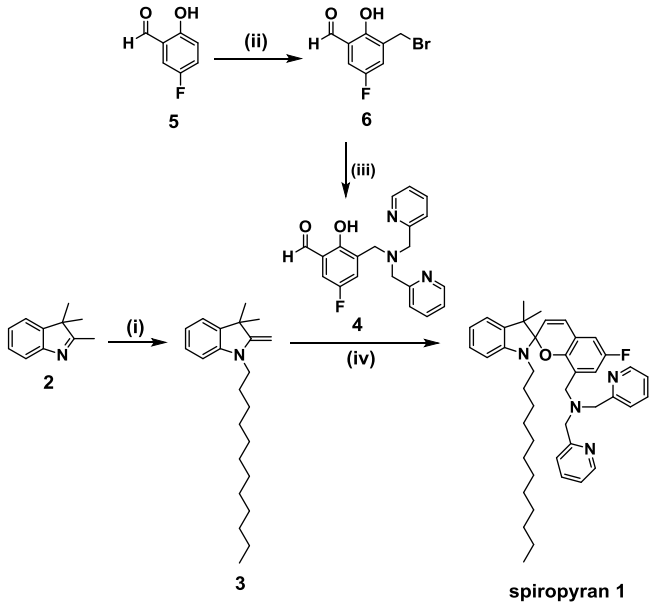

Scheme 1. Synthesis of Spiropyran **1**. (i) 1-Bromododecane, diisopropylethylamine, acetonitrile, reflux, 72 h, 60 %. (ii) paraformaldehyde, HBr, 70 °C, 18 h, 72%. (iii) bis(2-pyridylmethyl)amine, Et_3N, THF, reflux, 18 h, 60-70%. (iv) **4**, EtOH, reflux, 18 h, 20 %.

Spiropyran **1** (Figure 1) was designed to self-assemble into a micelle-like nanostructure in aqueous environment as depicted in Figure 1. A 6'-fluorine substituent was also incorporated to suppress undesired isomerization from SP to MC in the absence of Zn^{2+} in polar protic solvents,[2e] which would result in non-Zn^{2+} triggered and undesired release of the payload in aqueous media. The spiropyran has an appended hydrophopic tail to allow self-assembly into a micelle-like structure for trapping the payload within its core. The bis(2-pyridylmethyl)amine group was incorporated into the design to specifically coordinate Zn^{2+}.[15]

Spiropyran **1** was prepared as detailed in the Materials and Methods section and as depicted in Scheme 1. Briefly, base-catalysed alkylation of indolenine **2** with 1-bromododecane gave indoline **3**. Condensation of indoline **3** with aldehyde **4** gave spiropyran **1** in 20 % overall yield after purification by normal phase silica chromatography. Reaction of benzylic bromide **6** with bis(2-pyridylmethyl)amine gave compound **4**.[2e] Spiropyran-based nanocarriers were subsequently formed by mixing spiropyran **1** with 2-distearoyl-sn-glycero-3-phosphoethanolamine-N-carboxy(polyethylene glycol)-5000 and lecithin, to stabilise the nanostructure and prevent aggregation of the nanocarriers in aqueous solution.[16] The resultant mixture was nanoprecipitated[17, 18] into water and excess reagents were removed by centrifugation to yield the Zn^{2+} responsive nanocarriers as detailed in the ESI.

Physical and Optical Properties of Blank Spiropyran-based Nanocarriers (SpN).

The size distribution profile of the blank nanocarriers (**SpN**) was determined in solution in both the absence and presence of Zn^{2+} using dynamic light scattering (DLS). In the absence of Zn^{2+}, the size of **SpN** was determined to be approximately 575 nm. Particle diameter increased linearly with increasing Zn^{2+} concentrations up to ~720 nm in the presence of 5 mM added Zn^{2+} as shown in Figure 2A and detailed in the ESI. Binding to Zn^{2+} and associated switching from the SP isomer to the MC-Zn^{2+} complex, results in an expansion of **SpN**. This expansion then releases the encapsulated payload from the nanocarriers. In addition, **SpN** was assayed against a range of biologically relevant metal ions (K^+, Ce^+, Ni^{2+}, Fe^{2+}, Cu^{2+}, Na^+, Li^+, Zn^{2+}, Mg^{2+}, Ca^{2+} and Co^{2+}) to define its selectivity profile. The nanocarrier clearly shows excellent selectivity for Zn^{2+}, with none of the other tested metal ions showing any affinity (see Figure S8B).

Next, the spectroscopic properties of **SpN** in the absence of encapsulated payload, were explored by UV-vis and fluorescence spectroscopy. Addition of excess Zn^{2+} to **SpN** gave rise to strong absorbance (λ_{max} ~ 550 nm) and fluorescence (λ_{ex} = 532 nm, $\lambda_{em\ max}$ = ~ 660 nm) as shown in Figures 2B and C, respectively. This is consistent with the switching of spiropyran **1** from the colorless SP isomer to a more colored and fluorescent MC-Zn^{2+} complex.[12b, 17] Fluorescence of **SpN** treated with varying concentrations of Zn^{2+} (0-125 μM) was recorded to determine the detection limit. The lowest Zn^{2+} concentration required to switch the nanocarriers was found to be 6.25 μM (purple, Figure 2C), which is within the biologically relevant range.

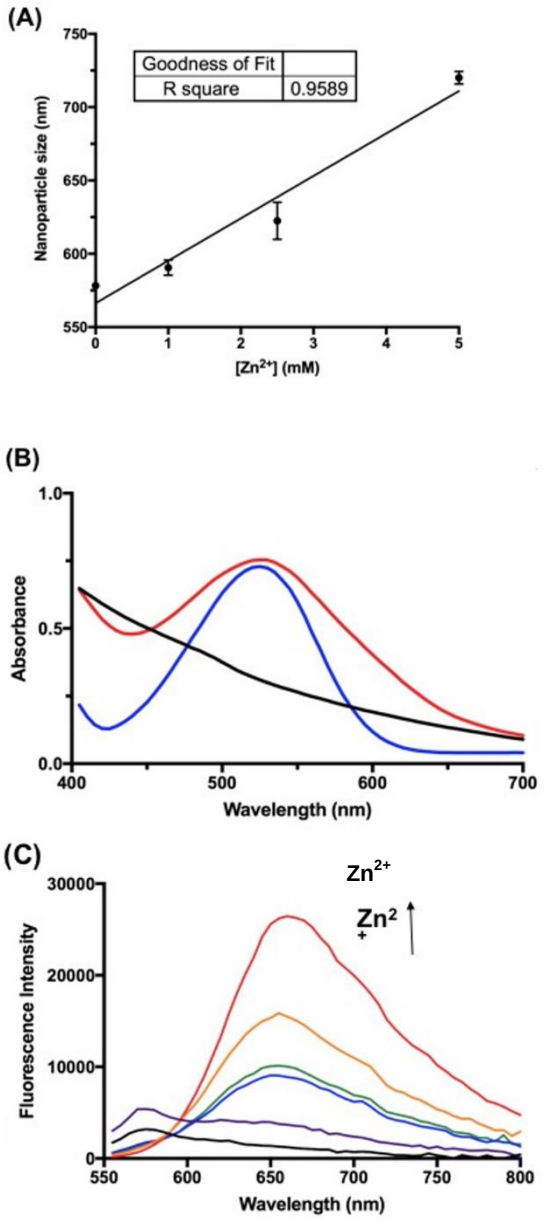

Figure 2. (A) Nanocarrier size distribution of **SpN** with increasing Zn^{2+} concentrations determined by dynamic light scattering. (B) Absorbance spectra of **SpN** in the absence of Zn^{2+} (black), **SpN** with 100 μM Zn^{2+} (red), and spiropyran **1** (50 μM) with 100 μM Zn^{2+} in acetonitrile (blue). (C) Fluorescence spectra of **SpN** with increasing Zn^{2+} concentrations at 0 μM (black), 6.25 μM (purple), 12.5 μM (blue), 31.25 μM (green), 62.5 μM (yellow) and 125 μM (red). The spectroscopy experiments were carried out in 96-well plates and absorbance / fluorescence were recorded using a plate reader. For the fluorescence experiments, the samples were excited at λ = 532 nm.

Payload Encapsulation and Its Zn^{2+} Triggered Release in Solution and in Cells.

The ability of the spiropyran-based nanocarrier to encapsulate and release coumarin- and pyrene-based fluorophores on binding to Zn^{2+} was investigated. 7-Hydroxycoumarin and 1-hydroxypyrene were chosen for initial study as their emission profiles (λ_{ex} ~ 320 nm, λ_{em} in the region of 300 – 450 nm) are separate, and hence readily distinguishable from the emission of the nanocarriers (λ_{em} = 660 nm). Nanocarriers with encapsulated payload were prepared by premixing spiropyran **1** with either 7-hydroxycoumarin (**cu)** or 1-hydroxypyrene (**py**). The resulting nanocarriers, referred to as **SpN-cu** and **SpN-py** respectively, were then nanoprecipitated in water (1 mL) as described before and detailed in the ESI.

Zn^{2+}-triggered release of 7-hydroxycoumarin from **SpN-cu** and 1-hydroxypyrene from **SpN-py** was investigated spectroscopically. In the absence of Zn^{2+}, fluorescence emission corresponding to the payload was not observed for samples containing either **SpN-cu** or **SpN-py** when excited at 320 nm (Figure 3A, blue). This suggests that, without added Zn^{2+}, the respective fluorophores remain trapped within the hydrophobic core of the nanocarriers. The lack of observed fluorescence is presumably due to aggregation-induced fluorescence quenching.[18] The addition of Zn^{2+} to a solution of **SpN-cu** gave rise to strong fluorescence at λ_{max} = 385 nm (λ_{ex} = 310 nm), characteristic of free 7-hydroxycoumarin (Figure 3A, black). The addition of Zn^{2+} to **SpN-py** gave a similar result, with the observed fluorescence signals at λ_{max} = 380 nm and 395 nm, characteristic of free 1-hydroxypyrene (Figure 3A, red). These experiments were repeated with varying Zn^{2+} concentrations as detailed in the ESI Figure S11, to reveal a linear relationship between added Zn^{2+} and fluorescence of released fluorophore. It is thus clear that Zn^{2+} triggers release of fluorophore from the nanocarrier. Additional experiments, such as time-based fluorescence and HPLC analyses are required to characterise the rate of payload release from **SpN**.

Next, the release of the encapsulated 7-hydroxycoumarin from **SpN-cu** in response to endogenous Zn^{2+} found in apoptotic HEK293 cells was investigated using confocal microscopy to measure the fluorescence of the released fluorophore and the Zn^{2+}-bound nanocarrier. Apoptosis is known to give rise to increased levels of free intracellular Zn^{2+} [13d] that can trigger the release of payload from the nanocarrier. **SpN-cu** was incubated with HEK293 cells treated with staurosporine to induce apoptosis.[19] Cells were carefully washed with PBS buffer to remove any extracellular nanocarriers and Zn^{2+}. Irradiation of these cells with the green laser from the confocal microscope activated the MC-Zn^{2+} complexes formed upon **SpN** binding with Zn^{2+}, giving rise to red fluorescence characteristic of this complex (Figure 3B and C, red channel). This allows easy tracking of the nanocarrier in apoptotic cells by confocal microscopy where intracellular Zn^{2+} concentration is elevated. Irradiation of the cells with the blue laser light resulted in blue fluorescence signal characteristic of released 7-

hydroxycoumarin (Figure 3B and C, blue channel). More importantly, the blue fluorescence corresponding to 7-hydroxycoumarin was observed by confocal microscopy in the same region of the microscope slide as the red-fluorescence, shown in Figures 3B and C (overlay), which indicates that the nanocarriers and 7-hydroxycoumarin are co-located. Further validation of the Zn^{2+}-triggered release of 7-hydroxycoumarin from **SpN-cu** was obtained by incubating **SpN-cu** with healthy cells lacking high levels of free Zn^{2+}. No red or blue fluorescence was observed for healthy cells without added staurosporine (Figure 3D) due to the absence of sufficient intracellular Zn^{2+} to switch **SpN-cu** and release the fluorophore. Finally, staurosporine and **SpN-cu** treated cells were subsequently incubated with a cell-permeable Zn^{2+} chelator N,N,N',N'-tetrakis(2-pyridylmethyl)ethylenediamine (TPEN) to dissociate Zn^{2+} from the MC-Zn^{2+} complex and switch the nanocarrier back to the non-fluorescent SP isomer. As expected, the red fluorescence signal of the nanocarrier inside the TPEN-treated cells (Figure 3F, red channel) is significantly lower than that observed and measured for cells without TPEN (Figure 3E, red channel and Figure 3G). The red fluorescence observed in Figure B and C is thus a result of Zn^{2+} binding to the nanocarrier. Collectively, these data demonstrate that formation of the MC-Zn^{2+} complex and subsequent Zn^{2+}-triggered release of the encapsulated 7-hydroxycoumarin from **SpN-cu** in cells is promoted by increased concentration of free intracellular Zn^{2+}, such as found in apoptotic cells.[20] Non-specifically release of the payload is thus not an issue.

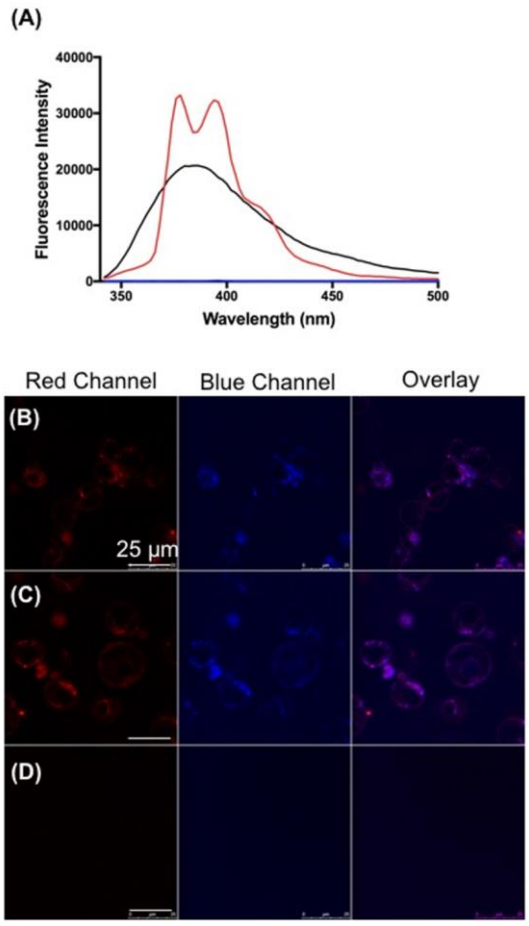

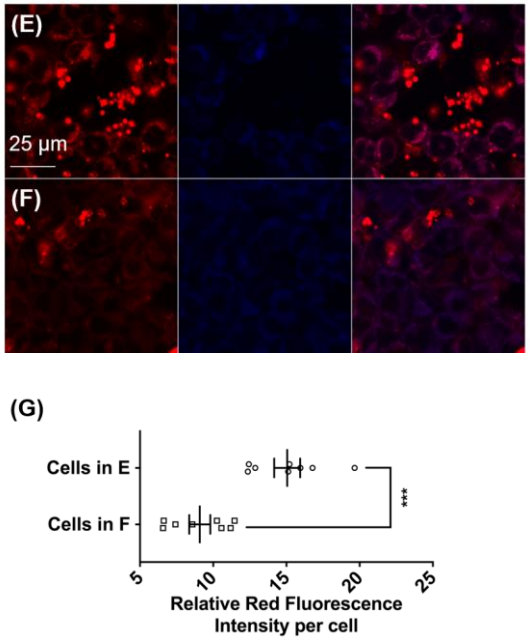

Figure 3. (A) Fluorescence spectra for **SpN-cu** (black) and **SpN-py** (red) with 200 μM Zn^{2+} respectively. Blue line represents fluorescence signal for **SpN-cu** and **SpN-py** in the absence of Zn^{2+}. The excitation wavelength for both **SpN-cu** and **SpN-py** was 320 nm. (B) – (F) Confocal microscope images of HEK293 cells (B) treated with 0.8 μM of staurosporine and **SpN-cu**; (C) treated with 1.6 μM of staurosporine and **SpN-cu** and (D) **SpN-cu** only, no staurosporine i.e. healthy cells; (E) same preparation of cells as (C) with image taken from different region of the microscope slide; (F) same preparation of cells from (C) with TPEN (50 μM) added to chelate and remove Zn^{2+} from the cells. For (B)-(F), red signals represent the fluorescence of MC-Zn^{2+} complex and blue signals represent the fluorescence of 7-hydroxycoumarin. Images (B)-(D) were captured with 20% gain and images (E)-(F) were captured with 50% gain. (G) Red fluorescent intensity in (E) and (F) were measured for 8 randomly chosen cells per image. Unpaired t test was used, *** represents p≤0.001.

Zn^{2+}-triggered Inhibition of Caspase Activity.

The use of spiropyran-based nanocarriers as a stimuli-responsive delivery tool was explored by encapsulating a caspase inhibitor and modulating caspase activity on its release in apoptotic cells in response to an increased intracellular Zn^{2+} level. Caspases (e.g. caspase-3, -6 and -9) are highly expressed in apoptotic cells,[21] and inhibition of these enzymes can potentially halt cellular damages and apoptosis.[6]

Spiropyran-based nanocarriers encapsulated with Azure B (**SpN-ab**, where **SpN** represents the nanocarriers and **–ab** Azure B), a potent inhibitor of caspase -3 and -6,[22] were prepared as detailed in the ESI. The sizes of **SpN-ab,** upon addition of 0-100 μM Zn^{2+}, was measured by dynamic light scattering as detailed in the ESI. Consistent with the blank nanocarrier (**SpN**), the size of **SpN-ab** increases linearly with increasing Zn^{2+} concentration (Figure S10, ESI). This suggests that binding with Zn^{2+} results in an expansion of **SpN-ab**,

allowing the release of the payload. **SpN-ab** was then assayed against purified recombinant human caspases-3 and -6 to investigate Zn^{2+}-triggered release of Azure B *in vitro.* Azure B is a known inhibitor for caspases-3 and -6 and thus both were assayed to demonstrate that inhibitory activity is not affected by the nanocarrier. In a typical caspase assay, **SpN-ab** was pre-incubated with varying Zn^{2+} concentrations as detailed in the ESI and each sample was incubated with either purified caspase-3 or -6 at 37 ^{o}C for 5 min in buffer containing EDTA (200 μM). Respective enzyme activity was determined by monitoring fluorescence of the cleaved AMC (amido-4-methylcoumarin) of fluorogenic enzyme substrates, Z-DEVD-AMC (caspase-3)[23] or Ac-VEID-AMC (caspase-6),[24] for 30 min at 37 ^{o}C. Azure B is released in a Zn^{2+} concentration dependent fashion from **SpN-ab** and this inhibited both caspase-3 (Figure 4A) and -6 (Figure 4B). Specifically, the proteolytic activity of both caspases decreased in response to increasing concentrations of Zn^{2+}, presumably the result of increasing Azure B payload release from **SpN-ab**. In contrast, **SpN-ab** does not inhibit either caspase-3 or -6 in the absence of Zn^{2+} (ESI). A control experiment where the enzymes were incubated with Zn^{2+} alone (500 μM, ESI) in the buffer containing EDTA (500 μM) demonstrates that Zn^{2+} does not inhibit caspase activity when chelated to EDTA and thus the observed inhibition is a result of controlled-release of Azure B from **SpN-ab** in the presence of Zn^{2+}.

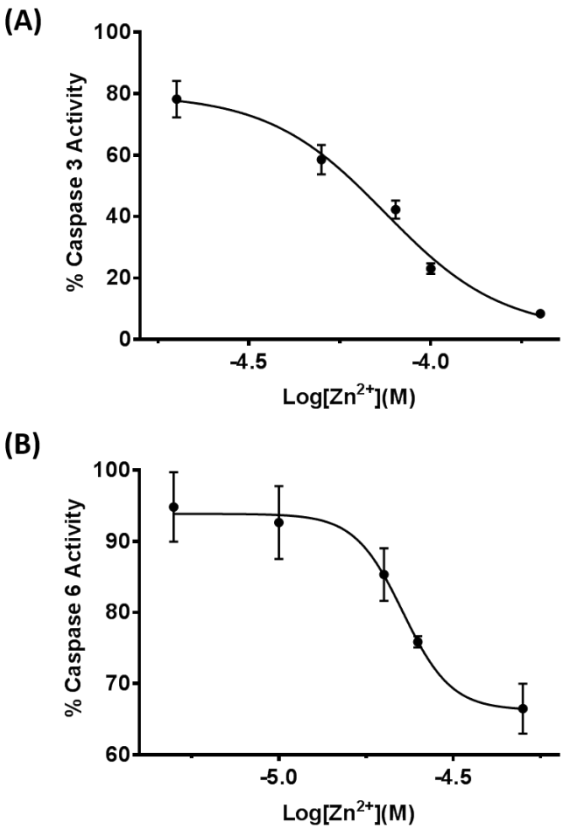

Figure 4. *In vitro* assays of purified human caspase-3 (A) and -6 (B) activity in the presence of **SpN-ab** and Zn^{2+} (0-200 μM). Each data point represents the rate of enzymatic cleavage of the respective fluorogenic substrate at the specified Zn^{2+} concentration over 30 min at 37 ^{o}C and normalised to untreated enzyme activity. Error bars represent the standard error of means calculated over three biological replicates.

Next, confocal cell imaging was performed to demonstrate the ability of **SpN-ab** to sense Zn^{2+} level and deliver payload in HEK293 cells. The binding of **SpN-ab** to intracellular Zn^{2+} released the encapsulated Azure B in apoptotic HEK293 cells, which led to decreased caspase activity. Green fluorescence of a commercially available caspase detection reagent,[25] produced from activity of caspases-3 and -7, was observed in the nuclei of HEK293 cells after 24 h-incubation with staurosporine (Figure 5A, green channel), with Hoescht 33258 staining to visualize and locate the nuclei. In contrast, lower green fluorescence was observed in the nuclei of non-treated cells (Figure 5B, Green Channel) due to minimal caspase activity in these cells, consistent with literature report.[21] HEK293 cells were then incubated with **SpN-ab** in the presence of staurosporine (3.2 μM) to demonstrate the nanocarrier's ability to deliver Azure B and inhibit caspase activity in cells. Images of these cells obtained by a confocal microscope showed red fluorescence characteristic of the MC-Zn^{2+} complex as observed previously in Figure 3. Critically, the intensity of intranuclear green fluorescence (Figure 5C and 5D), an indicator to cellular caspase activity, is 1.2-fold lower than cells without added **SpN-ab** (Figure 5A). These results clearly demonstrate the dual functionality of **SpN-ab** to deliver azure B to apoptotic cells in response to elevated Zn^{2+} levels and bring inhibition to intracellular caspase activity while providing a means to image the associated Zn^{2+} increase through the formation of the highly fluorescent MC-Zn^{2+} complex.

The delivery of azure B by **SpN-ab** and inhibition of caspase activity during cell apoptosis was further demonstrated real-time using time-lapsed live cell microscopy. Apoptotic cells were incubated with either **SpN-ab** (Figure 6A) or blank nanocarrier (**SpN**) (Figure 6B). Intranuclear green fluorescence emitted from the abovementioned caspase detection reagent ($\lambda_{ex/em}$ = 488 / 500-550 nm) was measured every 30 min over 20 h to monitor caspase-3 activity over time. A steady rise in overall fluorescence intensity was observed in cells treated with **SpN**, indicating an increase in caspase-3 activity caused by progression of apoptosis across the cell population. In comparison, the start of this fluorescence increase was delayed for 300 min in cells treated with **SpN-ab** (Figure 6C, red), a clear indication that the activation of caspase activity in these cells was postponed, presumably by the release of Azure B from **SpN-ab**. The ability of **SpN-ab** to mediate inhibition of caspase activity was further evidenced by a 34 % lower overall fluorescence in treated cells compared to cells incubated with **SpN** (Figure 6C, black). Collectively, these results represent the first real-time cell-based images that demonstrate the therapeutic effect of Azure B on caspase activity during apoptosis, where the release of the inhibitor is tightly controlled by levels of intracellular Zn^{2+} in dying cells.

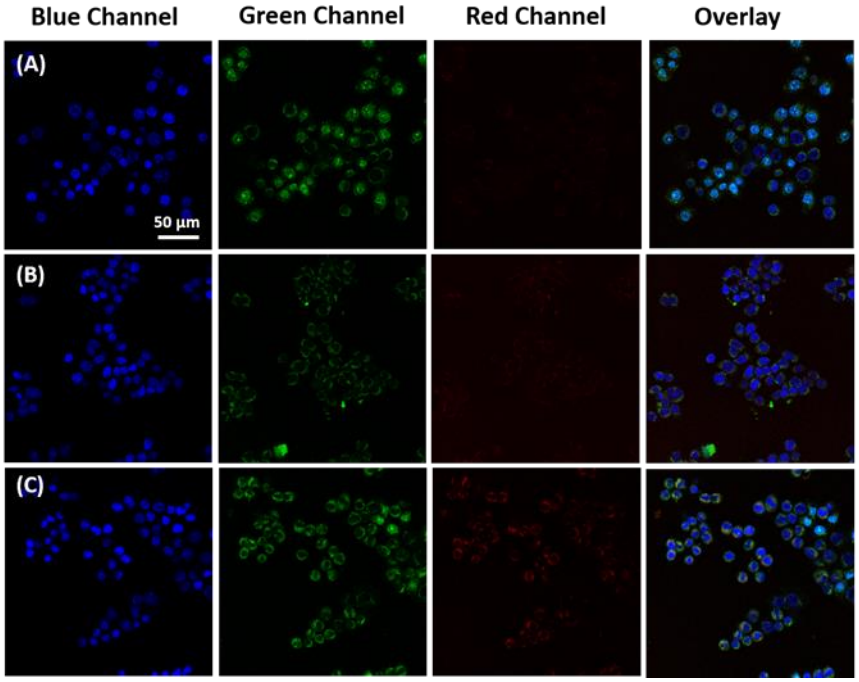

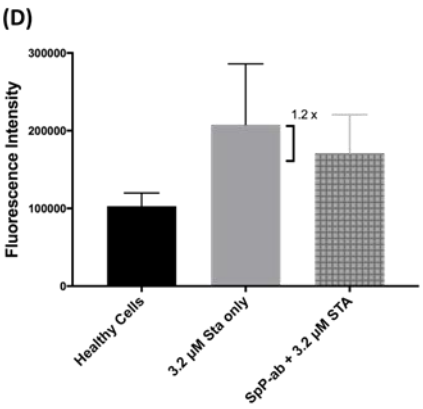

Figure 5A – D. Confocal images of HEK293 cells (A) incubated overnight with staurosporine (3.2 μM) only; (B) without added staurosporine; (C) incubated with staurosporine (3.2 μM) overnight followed by incubation with **SpN-ab** for 2 h. All the cells were stained with Hoescht 33258 and Cell Event caspase 3/7 green detection reagent. The blue, green and red channels represent fluorescence emissions recorded at Ex/Em=405 nm/ 410-475 nm, Ex/Em=488 nm/ 500-550 nm and Ex/Em=561 nm/ 570-750 nm, respectively. The three channels were overlaid using ImageJ to produce the 'overlay' images. Scale bares are 50 μm. (D) Graph showing relative fluorescence intensity of healthy cells (black), cells treated with staurosporine only (grey) and cells treated with both staurosporine and **SpN-ab** (grey checked). 20 randomly selected cells were measured for each treatment. Unpaired student t-test was used with $p<0.05$ (***).

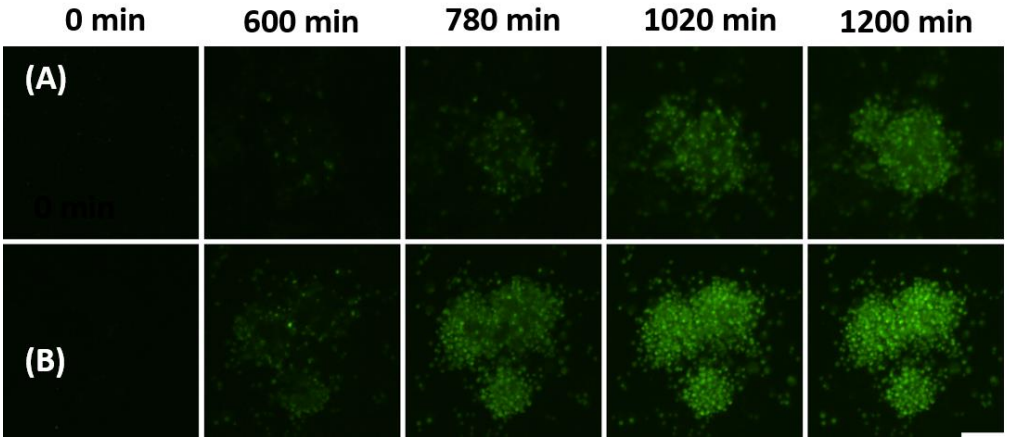

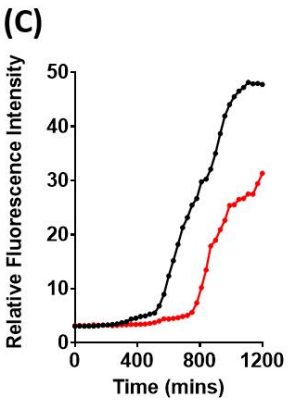

Figure 6. (A) HEK293 cells incubated with **SpN-ab**, staurosporine (3.2 μM) and CellEvent Caspase 3/7 green detection reagent and imaged every 30 min for 20 h; (B) HEK293 cells incubated with staurosporine (3.2 μM) and caspase detection reagent and imaged every 30 min for 20 h. All cells were imaged at Ex/Em = 488 / 500-550 nm. The images presented herein are taken at time points 0, 600, 780, 1020 and 1200 min. The scale bar represents 100 μm. (C) Relative fluorescence intensity measured from images (A) red and (B) black graph by ImageJ over 1200 min.

Zn^{2+}-triggered Inhibition of the 20S Proteasome Activity.

The ability of the nanocarriers to deliver a proteasome inhibitor to breast carcinoma cell line models was next investigated. The proteasome is an important therapeutic target in the treatment of cancers, but most proteasome inhibitors produce dose-limiting cytotoxicity to non-malignant cells that preclude their widespread clinical use.[26] With this in mind, a potent proteasome inhibitor, **5**[27] (Figure 7A insert), was encapsulated inside the nanocarriers for release in breast cancer cells reported to possess high levels of Zn^{2+}.[11] This provides potential to reduce cytotoxicity to non-malignant cells. This inhibitor was chosen due to its low nanomolar inhibition of the chymotrypsin-like (CT-L) subunit of the 20S proteasome, which is known to be upregulated in breast cancer and multiple myeloma.[27]

Nanocarriers encapsulated with inhibitor **5** (**SpN-5**), were prepared as detailed in the ESI. **SpN-5** was first assayed against purified rabbit 20S proteasome to investigate its ability to release the payload and inhibit the proteasome upon binding to Zn^{2+}. Briefly, **SpN-5** was pre-incubated with varying concentrations of Zn^{2+} (0-200 μM) overnight at ambient temperature to release the inhibitor based on the earlier studies. Purified 20S proteasome and a fluorogenic substrate, Suc-LLVY-AMC, specific for the CT-L subunit, were added to determine the enzymatic activity by fluorescence. Compound **5** released from **SpN-5** inhibited the

20S proteasome in a dose-dependent manner relative to Zn^{2+} concentration, as shown in Figure 7A. Specifically, the activity of the CT-L subunit of the 20S proteasome decreased with increasing concentrations of Zn^{2+} added to **SpN-5**. In contrast, proteasome incubated with **SpN-5** in the absence of Zn^{2+} only exhibited minimal inhibition (Figure 7B). A control experiment where the proteasome was treated with the blank nanocarrier **SpN** showed no inhibition of proteasome activity, either in the presence or absence of Zn^{2+} (Figure 7B). Collectively, these experiments demonstrate that blank nanocarriers, or Zn^{2+} alone, does not alter enzyme activity. Thus the observed inhibition of the CT-L subunit is a result of the release of compound **5** from **SpN-5** upon binding with Zn^{2+}.

Next, the ability of **SpN-5** to release inhibitor **5** in living cancer cells in response to added Zn^{2+} was demonstrated in a cell viability assay using two breast carcinoma cell lines, T47D and MDA-MB-468. Cells were seeded in a 96-well plate and incubated with **SpN-5** for 4 h to allow uptake of the nanocarriers. The cells were carefully washed with PBS buffer to remove excess nanocarriers and incubated with Zn^{2+} in the form of $Zn(ClO_4)_2$•$6H_2O$ and zinc pyrithione (1 eq.) for 24 h at 37 °C, to allow Zn^{2+} uptake into the cells. Cell viability was then measured for each treatment group by CellTitre-Glo luminescent assay as detailed in the ESI and normalised to the viability of the untreated cells as shown in Figure 8. Cells treated with **SpN-5** and 50 μM Zn^{2+} have significantly decreased viability (2 % and 14 % for T47D and MDA-MD-468 respectively). In contrast, cells treated with **SpN-5** in the absence of Zn^{2+} showed no cytotoxicity to both cancer cell lines. Similarly, no cytotoxicity was observed for cells treated with Zn^{2+} and zinc pyrithione (both 100 μM) in the absence of **SpN-5**. Thus, the observed cytotoxicity for **SpN-5** and Zn^{2+} treated cells is triggered by the release of inhibitor **5** from **SpN-5** upon binding to Zn^{2+}. Collectively, the results of the purified enzyme assay and the cell viability assay clearly demonstrate the ability of the nanocarriers to deliver an inhibitor drug into cancer cells in a Zn^{2+}-responsive manner. This provides an important first step toward cancer cell selective chemotherapy where the encapsulated drug is only delivered in tumorous cells with an elevated Zn^{2+} level, thus reducing cytotoxicity to normal cells. Further adjustment to the structure and composition of the nanocarrier is, however, needed to increase sensitivity to Zn^{2+} and produce a delivery system that responds to endogenous changes of Zn^{2+} concentrations in cancer cells.

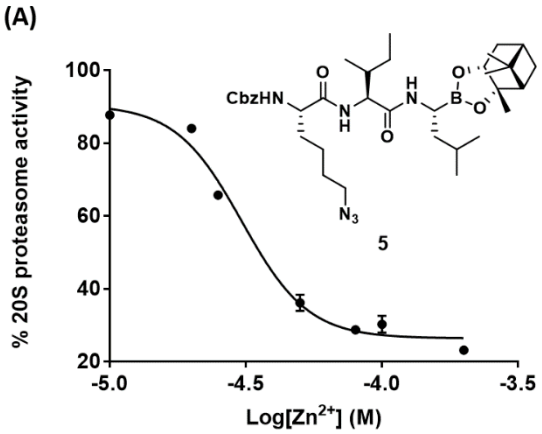

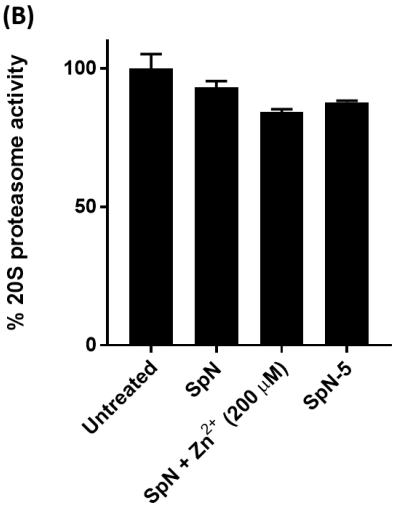

Figure 7. (A) *In vitro* assay of the 20S proteasome activity in the presence of **SpN-5** and Zn^{2+} (0-200 μM). Each data point represents the rate of enzymatic cleavage of the fluorogenic substrate Suc-LLVY-AMC at the specified Zn^{2+} concentration over 120 min at 37 °C normalised to sample without nanocarrier and Zn^{2+}. Insert: the structure of inhibitor **5**. (B) Proteasome activity upon treatment with the blank nanocarrier **SpN** with and without added Zn^{2+} (200 μM) or **SpN-5** in the absence of Zn^{2+}. Each bar represents the activity of the 20S proteasome in a specified treatment group normalised to the activity of the untreated proteasome. All error bars represent the standard error of means calculated over three biological replicates.

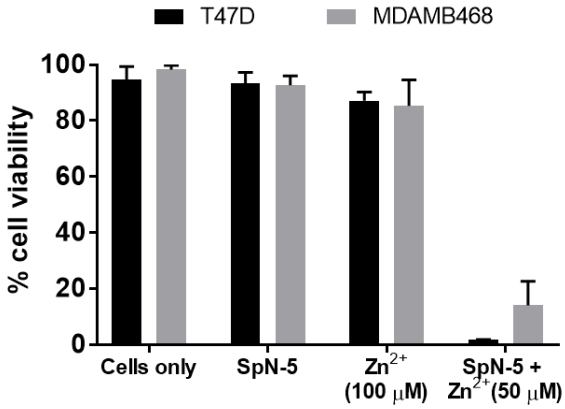

Figure 8. Cytotoxicity of **SpN-5** on breast cancer cell lines T47D (black bars) and MDAMB468 (grey bars). Each bar represents the viability of cells in the specified treatment group normalised to viability of untreated cells. Zn^{2+} was introduced in the form of $Zn(ClO_4)_2$•$6H_2O$ and 1 eq. of zinc pyrithione was used to allow Zn^{2+} to penetrate the cell membrane. Cell viability was measured using CellTiter-Glo luminescent cell viability assay. Error bars represent the standard error of means calculated over three biological replicates.

Conclusions

Here, we present a self-assembled spiropyran-based nanocarrier for payload encapsulation as a first step towards a stimuli-responsive delivery tool. Blank nanocarrier (**SpN**) was shown to coordinate Zn^{2+} with the appended bis(2-pyridylmethyl)amine group, which switches the nanocarrier from the SP state to the MC-Zn^{2+} complex. This results in a linear increase in the fluorescence of the MC-Zn^{2+} complex (λ_{em} = 660 nm) with increasing Zn^{2+} concentration (6.25 µM – 125 µM). This system was then used to encapsulate two organic fluorophores, 7-hydroxycoumarin (**SpN-cu**) and 1-hydroxypyrene (**SpN-py**). The Zn^{2+}-triggered release of coumarin and pyrene from the nanocarriers in solution was demonstrated by fluorescence spectroscopy, where an increase in fluorescence of the released fluorophore was observed with increasing Zn^{2+} concentration. This was further validated by confocal microscopic images of HEK293 cells that showed the fluorescence of MC-Zn^{2+} complexes and the released fluorophores was co-located in cells. The observed fluorescence of the MC-Zn^{2+} complex also allows tracking of the intracellular distribution of the nanocarrier. A caspase inhibitor, Azure B, was encapsulated into the nanocarrier (**SpN-ab**) and released in aqueous solution in response to increasing Zn^{2+} concentration (0 - 200 µM) to inhibit caspase activity both in solution and in apoptotic cells. Time-lapsed confocal microscopy further validated that caspase activity was inhibited by Azure B released by the nanocarrier in real-time during apoptosis. This provides an important basis for a tool that inhibits caspase activity specifically when apoptosis is triggered and could potentially affect the rate of apoptosis. Furthermore, the nanocarriers were shown to encapsulate and release a small-molecule proteasome inhibitor (**SpN-5**) upon binding with Zn^{2+} (0 - 200 µM) to inhibit purified 20S proteasome. Treatment of breast cancer cell lines with **SpN-5** and Zn^{2+} (50 µM) induced significant cytotoxicity, while **SpN-5** alone was shown to be non-cytotoxic. This clearly demonstrates the ability of the nanocarrier to deliver a fully functional inhibitor drug into cancer cells in a Zn^{2+}-responsive manner. More importantly, spiropyrans can be readily coupled with a range of molecules to This versatility represents a significant and high impact advancement to a smart platform for specific disease marker mediated drug delivery and more widely for regulation of marker promoted cellular events.

Experimental Section

General

Unless otherwise indicated, all starting materials, chemicals and anhydrous solvents were purchased from Sigma–Aldrich (USA) and were used without further purification. UNIBOND C-18 reverse phase silica gel was purchased from Analtech Inc. (USA). Compound **4** was prepared as shown in Scheme 1, as previously described.[2e] ^{1}H and ^{13}C NMR spectra were recorded on a Varian 500 MHz and a Varian Inova 600 MHz instruments in the indicated solvents. Chemical shifts are reported in ppm (δ). Signals are reported as s (singlet), brs (broad singlet), d (doublet), dd (doublet of doublets), t (triplet) or m (multiplet). High-resolution mass spectra were collected using an LTQ Orbitrap XL ETD with flow injection, with a flow rate of 5 µL min^{-1}. All graphs were generated using GraphPad Prism 7 and IgorPro 6.

1-Dodecyl-3,3-dimethyl-2-methyleneindoline (3).

2,3,3-Trimethylindolenine **2** (500 mg, 3.14 mmol), 1-bromododecane (1.5 mL, 6.24 mmol) and DIPEA (1.1 mL, 6.24 mmol) were dissolved in anhydrous acetonitrile (10 mL) and set to reflux for 72 h. Excess solvent was removed under vacuum. The crude reaction mixture was purified using normal phase silica gel (0 – 3 % ethyl acetate in hexane) to yield **3** as a red, viscous liquid (770 mg, 60 %). ^{1}H NMR (500 MHz, $CDCl_3$) δ 7.13 – 7.07 (m, 2H), 6.74 (t, J = 7.5 Hz, 1H), 6.52 (d, J = 8.0 Hz, 1H), 3.85 (s, 1H), 3.82 (s, 1H), 3.47 (t, J = 7.3 Hz, 2H), 3.39 (t, J = 6.8 Hz, 1H), 1.65 – 1.53 (m, 3H), 1.33 – 1.25 (m, overlapped with H_2O peak from NMR solvent), 0.88 (t, J = 5.0 Hz, 3H); ^{13}C NMR (126 MHz, $CDCl_3$) δ 161.8, 146.2, 137.7, 127.6, 121.9, 18.3, 105.2, 72.9, 71.1, 44.3, 42.5, 32.1, 30.2, 27.4, 29.8 – 29.4 (4C), 26.4, 26.2, 22.9, 14.3. ESI (m/z) for $[C_{23}H_{37}N] + H^+$ calculated 328.29, found 328.30.

1-(1'-Dodecyl-6-fluoro-3',3'-dimethylspiro[chromene-2,2'-indolin]-8-yl)-N,N-bis(pyridin-2-ylmethyl)methanamine (Spiropyran 1).

Compound **3** (196 mg, 0.6 mmol) and compound **4** (220 mg, 0.6 mmol) were dissolved in anhydrous ethanol (10 mL) and the mixture was refluxed for 18 h. Excess solvent was removed under vacuo. The crude reaction mixture was purified using normal phase silica gel (0 – 7 % ethyl acetate in hexane) to give spiropyran **1** as a yellow, viscous liquid (80 mg, 20 %). ^{1}H NMR (500 MHz, $CDCl_3$) δ 8.47 (apparent d, J = 4.5 Hz, 2H), 7.60 – 7.57 (m, 2H), 7.46 – 7.45 (m, 2H), 7.16 (dd, J = 9.5, 2.5 Hz, 1H), 7.13 – 7.09 (m, 3H), 7.03 (d, J = 7.0 Hz, 1H), 6.80 (t, J = 7.5 Hz, 1H), 6.73 (d, J = 10.0 Hz, 1H), 6.65 (dd, J = 8.0, 3.5 Hz, 1H), 6.46 (d, J = 8.0 Hz, 1H), 5.73 (d, J = 10.0 Hz, 1H), 3.66 (s, 4H), 3.45 (dd, J = 29.5, 15.5 Hz, 2H), 3.14 – 3.08 (m, 1H), 3.03 – 2.97 (m, 1H), 1.60 – 1.45 (m, 3H), 1.29 – 1.15 (m, overlapped with H_2O peak), 0.88 (t, J = 6.5 Hz, 3H); ^{13}C NMR (126 MHz, $CDCl_3$) δ 159.7, 157.6, 155.7, 149.1, 148.2, 147.5, 137.1, 136.6, 136.5, 128.6, 127.6, 127.0, 126.9, 123.3, 122.7, 122.6, 122.0, 121.6, 121.5, 119.3, 118.8, 116.4, 116.2, 111.6, 111.4, 106.4, 104.8, 60.2, 59.2, 52.0, 51.1, 43.8, 32.1, 29.9 – 29.8 (m), 29.6, 2 x 29.5, 29.2, 27.5, 26.1, 22.9, 20.5, 14.3. HRMS (m/z) for $[C_{43}H_{53}FN_4O] + Na^+$ calculated 683.4096, found 683.4092.

Acknowledgements

The authors acknowledge funding from the Centre for Nanoscale BioPhotonics (CNBP), through the Australian Research Council (ARC) CE140100003. This work was performed in part at the OptoFab node of the Australian National Fabrication Facility (ANFF) utilizing Commonwealth and South Australian State Government Funding. The authors also acknowledge Dr. Agatha Labrinidis and the Adelaide Microscopy core facility for confocal access.

Keywords: spiropyran-based nanocarrier • metal ions • apoptosis • payload delivery • fluorescence

[1] Y. Wang, J. Y. J. Shyy and S. Chien in *Fluorescence Live-Cell Imaging: Principles and Applications in Mechanobiology*, Eds.: G. M. Artmann and S. Chien), Springer Berlin Heidelberg, Berlin, Heidelberg, **2008**, pp. 65-84.
[2] a) S. Heng, C. A. McDevitt, D. B. Stubing, J. J. Whittall, J. G. Thompson, T. K. Engler, A. D. Abell and T. M. Monro, *Biomacromol.* **2013**, *14*, 3376-3379; b) S. Heng, M.-C. Nguyen, R. Kostecki, T. M. Monro and A. D. Abell, *RSC Adv.* **2013**, *3*, 8308-8317; c) S. Heng, A. M. Mak, R. Kostecki, X. Zhang, J. Pei, D. B. Stubing, H. Ebendorff-Heidepriem and A. D. Abell, *Sensor. Actuator. B-Chem.*

2017, *252*, 965-972; d) S. Heng, C. A. McDevitt, R. Kostecki, J. R. Morey, B. A. Eijkelkamp, H. Ebendorff-Heidepriem, T. M. Monro and A. D. Abell, *ACS Appl. Mater. Inter.* **2016**, *8*, 12727-12732; e) S. Heng, P. Reineck, A. K. Vidanapathirana, B. J. Pullen, D. W. Drumm, L. J. Ritter, N. Schwarz, C. S. Bonder, P. J. Psaltis, J. G. Thompson, B. C. Gibson, S. J. Nicholls and A. D. Abell, *ACS Omega* **2017**, *2*, 6201-6210.
[3] a) M. Purdey, J. Thompson, T. Monro, A. Abell and E. Schartner, *Sensors* **2015**, *15*, 29893; b) M. S. Purdey, H. J. McLennan, M. L. Sutton-McDowall, D. W. Drumm, X. Zhang, P. K. Capon, S. Heng, J. G. Thompson and A. D. Abell, *Sensor. Actuator. B-Chem.* **2018**, *262*, 750-757; c) S. Heng, X. Zhang, J. Pei and A. D. Abell, *Biosensors* **2017**, *7*.
[4] X. Zhang, S. Heng and A. D. Abell, *Chem. Eur. J.* **2015**, *21*, 10703-10713.
[5] a) N. Schrantz, M. T. Auffredou, M. F. Bourgeade, L. Besnault, G. Leca and A. Vazquez, *Cell Death Differ.* **2001**, *8*, 152; b) S. J. Eron, D. J. MacPherson, K. B. Dagbay and J. A. Hardy, *ACS Chem. Biol.* **2018**, *13*, 1279-1290.
[6] A. G. Daniel, E. J. Peterson and N. P. Farrell, *Angew. Chem. Int. Ed.* **2014**, *53*, 4098-4101.
[7] a) J. M. Brown and L. D. Attardi, *Nat Rev Cancer* **2005**, *5*, 231-237; b) H. Okada and T. W. Mak, *Nat. Rev. Cancer* **2004**, *4*, 592-603.
[8] L. A. O'Reilly and A. Strasser, *Inflamm. Res.* **1999**, *48*, 5-21.
[9] a) S. Shimohama, *Apoptosis* **2000**, *5*, 9-16; b) M. Vila and S. Przedborski, *Nat. Rev. Neurosci.* **2003**, *4*, 365-375.
[10] F. Larner, L. N. Woodley, S. Shousha, A. Moyes, E. Humphreys-Williams, S. Strekopytov, A. N. Halliday, M. Rehkamper and R. C. Coombes, *Metallomics* **2015**, *7*, 112-117.
[11] P. Chandler, B. S. Kochupurakkal, S. Alam, A. L. Richardson, D. I. Soybel and S. L. Kelleher, *Mol. Cancer* **2016**, *15*, 2.
[12] a) S. Heng, C. A. McDevitt, R. Kostecki, J. R. Morey, B. A. Eijkelkamp, H. Ebendorff-Heidepriem, T. M. Monro and A. D. Abell, *ACS Appl. Mater. Inter.* **2016**, *8*, 12727-12732; b) P. Rivera-Fuentes and S. J. Lippard, *ChemMedChem* **2014**, *9*, 1238-1243.
[13] a) P. Zalewski, A. Truong-Tran, S. Lincoln, D. Ward, A. Shankar, P. Coyle, L. Jayaram, A. Copley, D. Grosser, C. Murgia, C. Lang and R. Ruffin, *Biotechniques* **2006**, *40*, 509-520; b) J. L. Major, G. Parigi, C. Luchinat and T. J. Meade, *Proc. Nat. Acad. Sci.* **2007**, *104*, 13881; c) P. Chandler, B. S. Kochupurakkal, S. Alam, A. L. Richardson, D. I. Soybel and S. L. Kelleher, *Mol. Cancer* **2016**, *15*, 2. d) R. B. Franklin, L. C. Costello, *J. Cell. Biochem.* **2009,** *106,* 750.
[14] a) C. F. Cheok, *Cell Cycle* **2012**, *11*, 2227-2227; b) R. V. J. Chari, *Acc. Chem. Res.* **2008**, *41*, 98-107.
[15] a) J. M. K. Kwong, C. Hoang, R. T. Dukes, R. W. Yee, B. D. Gray, K. Y. Pak and J. Caprioli, *Invest. Ophth. Vis. Sci.* **2014**, *55*, 4913-4921; b) J. Glerup, P. A. Goodson, D. J. Hodgson, K. Michelsen, K. M. Nielsen and H. Weihe, *Inorg. Chem.* **1992**, *31*, 4611-4616; c) F.-Y. Wu, F.-Y. Xie, Y.-M. Wu and J.-I. Hong, *Spectrochimica Acta Part A: Molecular and Biomolecular Spectroscopy* **2008**, *70*, 1127-1133; d) G. Liu, K. Y. Choi, A. Bhirde, M. Swierczewska, J. Yin, S. W. Lee, J. H. Park, J. I. Hong, J. Xie, G. Niu, D. O. Kiesewetter, S. Lee and X. Chen, *Angew. Chem. Int. Ed.* **2011**, *51*, 445-449.
[16] J. M. Chan, L. Zhang, K. P. Yuet, G. Liao, J.-W. Rhee, R. Langer and O. C. Farokhzad, *Biomaterials* **2009**, *30*, 1627-1634.
[17] S. Heng, C. A. McDevitt, D. B. Stubing, J. J. Whittall, J. G. Thompson, T. K. Engler, A. D. Abell and T. M. Monro, *Biomacromol.* **2013**, *14*, 3376-3379.
[18] Y. J. Wang, Z. Y. Li, J. Q. Tong, X. Y. Shen, A. J. Qin, J. Z. Sun and B. Z. Tang, *J. Mater. Chem. C* **2015**, *3*, 3559-3568.
[19] C. A. Belmokhtar, J. Hillion and E. Segal-Bendirdjian, *Oncogene* **2001**, *20*, 3354-3362.
[20] D. K. Perry, M. J. Smyth, H. R. Stennicke, G. S. Salvesen, P. Duriez, G. G. Poirier and Y. A. Hannun, *J. Biol. Chem.* **1997**, *272*, 18530-18533.
[21] D. R. McIlwain, T. Berger and T. W. Mak, *CSH Perspect. Biol.* **2013**, *5*, a008656.
[22] P. Pakavathkumar, G. Sharma, V. Kaushal, B. Foveau and A. C. LeBlanc, *Sci. Rep.* **2015**, *5*.
[23] S. Mohr, B. Zech, E. G. Lapetina and B. Brune, *Biochem. Biophys. Res. Commun.* **1997**, *238*, 387-391.
[24] R. V. Talanian, C. Quinlan, S. Trautz, M. C. Hackett, J. A. Mankovich, D. Banach, T. Ghayur, K. D. Brady and W. W. Wong, *J. Biol. Chem.* **1997**, *272*, 9677-9682.
[25] T. C. Huang, J. F. Lee and J. Y. Chen, *Mar. Drugs.* **2011**, *9*, 1995-2009.
[26] a) A. Field-Smith, Morgan, J. G., Davies, F. E., *Ther. Clin. Risk Manag.* **2006**, *2*, 271-279; b) R. Z. Orlowski and D. J. Kuhn, *Clin. Cancer Res.* **2008**, *14*, 1649-1657.
[27] X. Zhang, A. Adwal, A. G. Turner, D. F. Callen and A. D. Abell, *ACS Med. Chem. Lett.* **2016**.

Entry for the Table of Contents (Please choose one layout)

Layout 2:

FULL PAPER

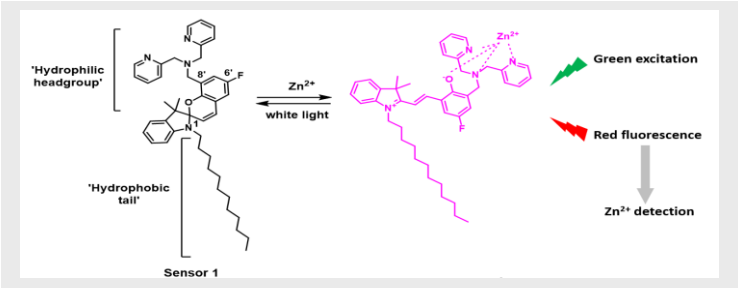

Here we present the first account of a Zn^{2+}-responsive delivery tool with added sensing and imaging capabilities. The delivery system consists of a spiropyran with an appended hydrophobic tail to allow self-assembly into a micelle-like structure that is shown to encapsulate payloads, e.g. fluorophores and protease inhibitors, and release them in response to increased intracellular Zn^{2+} levels.

*Sabrina Heng, Xiaozhou Zhang, Jinxin Pei, Alaknanda Adwal, Philipp Reineck, Brant C. Gibson, Mark R. Hutchinson, Andrew D. Abell.**

Page No. 1 – Page No. 9

Title: Spiropyran-based Nanocarrier: A New Zn^{2+}-Responsive Payload Releasing System with Real Time Intracellular Sensing Capabilities.

Author/s:
Heng, S; Zhang, X; Pei, J; Adwal, A; Reineck, P; Gibson, BC; Hutchinson, MR; Abell, AD

Title:
Spiropyran-Based Nanocarrier: A New Zn2+-Responsive Delivery System with Real-Time Intracellular Sensing Capabilities

Date:
2019-01-14

Citation:
Heng, S., Zhang, X., Pei, J., Adwal, A., Reineck, P., Gibson, B. C., Hutchinson, M. R. & Abell, A. D. (2019). Spiropyran-Based Nanocarrier: A New Zn2+-Responsive Delivery System with Real-Time Intracellular Sensing Capabilities. CHEMISTRY-A EUROPEAN JOURNAL, 25 (3), pp.854-862. https://doi.org/10.1002/chem.201804816.